Analysis of galvanomagnetic measurements in intrinsic tellurium

François Gros d'Aillon* and C. H. Champness
Electrical Engineering Department, McGill University, P.O. Box 6070, Montreal, Quebec, Canada, H3C 3G1
(Received 18 June 1974)

Measurements of electrical conductivity (σ), Hall coefficient (R_H) and transverse magnetoresistance ($\Delta\rho/\rho_0$) have been made on intrinsic single-crystal tellurium samples from room temperature to about 600 K. No difference in R_H or $\Delta\rho/\rho_0$ was found between the orientations with current parallel or perpendicular to the c axis and no anisotropic shift of the anomalous Hall reversal temperature was observed. The results, as a function of temperature, were analyzed on a double-conduction-band model and a double-valence-band model. With the assumption of temperature-independent mobility ratios, ranges of possible values were determined. Using a computer program with certain rejection conditions, it was possible to narrow down further the mobility ratios for the double-conduction-band model and obtain an estimate of the energy separation between the two conduction bands. The double-valence-band model was found inapplicable in the intrinsic region, since it gave too steep a mobility decrease with temperature and too large a deviation from the extrapolated intrinsic carrier concentration.

I. INTRODUCTION

The anomalous sign reversal of the Hall coefficient in intrinsic tellurium, which takes place at about 514 K, was first reported by Wold[1] in 1916, but it is still not explained to the satisfaction of many workers. However, at least one of the earlier theories,[2] that of thermally generated acceptors arising from imperfections, has now been effectively ruled out by the fast-heating experiments across the transition temperature of Link and Lutsch.[3] The anomaly is now generally accepted to be a consequence of band structure. Two models have been proposed which qualitatively explain the two reversals, normal and anomalous, of Hall coefficient. These are (a) a double-conduction-band model with a higher band of lower mobility than the normal conduction band or (b) a double-valence-band model with a lower band of higher mobility than the normal valence band.

From an analysis of measured conductivity, Hall coefficient, and Seebeck coefficient, Rigaux[4] showed that a double-valence-band model could not explain the variation of Seebeck coefficient, which also shows an anomalous sign reversal, but at about 450 K. This was confirmed in a detailed analysis of similar data by Link.[5] He concluded that, with a double-conduction-band model, the mobility in the upper band should be essentially zero.

These conclusions appear to be in contradiction to the fact that a two-band structure is now well established for the valence band in tellurium. The two bands are separated by about 0.1 eV and give rise to the absorption band near 11 μm. In fact, this structure was considered by McKay and Gravelle[6] and by Grosse[7] to be the cause of the anomalous Hall-coefficient inversion.

In view of these conflicting conclusions, the present studies were undertaken to obtain further experimental evidence to support one or other of the two band models. The conduction band is not as easily studied experimentally as the valence band, since extrinsic n-type tellurium has never been prepared. Hence the studies of transport properties for this purpose must be obtained in the intrinsic range. Electrical conductivity, Hall coefficient, and transverse magnetoresistance measurements were therefore made on intrinsic single-crystal tellurium samples from room temperature to about 600 K, and the results were analyzed on the basis of the two band models. With certain simplifying assumptions and conditions, the model giving the more realistic conduction properties was then refined.

The zone-refined tellurium used had a "normal" Hall reversal temperature below 200 K, and by this criterion the purity of the samples used was higher than that in previous measurements of this kind. (Fukuroi et al.[8]: 230-280 K; Rigaux[4]: 345 K.) Furthermore, the transverse magnetoresistance measurements were the first set of such data taken on unequivocally single-crystal samples over the temperature range involved. In addition, the well-known sensitivity of transport properties to imperfections in tellurium arising from cutting and handling was not a problem in this work, because the samples were fully intrinsic over the whole range of measurement.

II. MEASUREMENTS

A. Experimental details

The transport measurements were carried out on nine samples of approximate dimensions 15 $\times 2 \times 1$ mm cut from a single crystal grown from

high-purity zone-refined tellurium. The long dimension (current axis) was cut parallel to the c direction in seven of the samples and perpendicular to it for the other two. The samples were etched for 2–3 min in a solution of composition $CrO_3 : HCl : H_2O$ in the ratio of 1 : 1 : 2 by weight to remove the surface layer.

The potential readings for the transport coefficients were taken from two pairs of wire probes on either side of the sample. Figure 1(a) shows the orientation of the magnetic field with respect to the crystal axes for the c-axis samples, and Fig. 1(b) shows that for the a-axis samples. A holder containing the sample was located between the poles of a conventional electromagnet, and the temperature of the sample was controlled by an electrically heated oil bath.

B. Experimental results

Initial experiments at room temperature showed the Hall voltage to be a linear function and the transverse magnetoresistance a quadratic function of magnetic induction B, at least up to 20 kG. However, most of the measurements were carried out at 10 kG. Figures 2–4 show the measured values of electrical resistivity, Hall coefficient, and transverse magnetoresistance as a function of temperature. The resistivity shows roughly a 1 to 2 ratio between samples with current parallel and perpendicular to the c axis, but no anisotropy is apparent in Hall coefficient and magnetoresistance. In particular, there is no detectable shift in the anomalous Hall-inversion temperature between the two orientations. Often magnetoresistance shows a maximum when the Hall effect vanishes, but in Fig. 4 no discernible maximum is apparent at the anomalous inversion temperature.

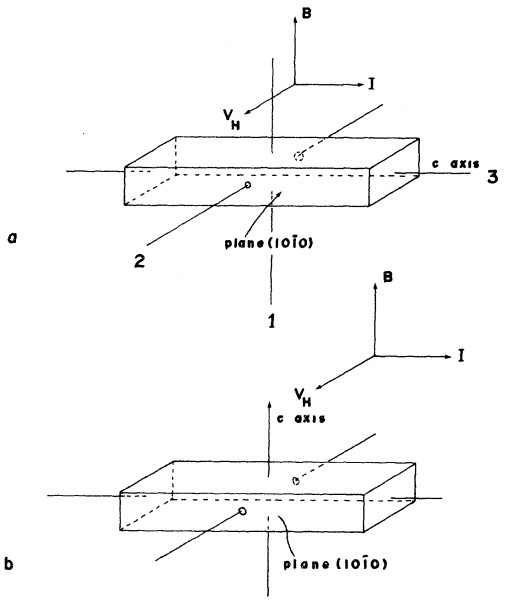

FIG. 1. Sample configurations used in the measurements. (a) Current parallel to c axis. (b) Current perpendicular to c axis.

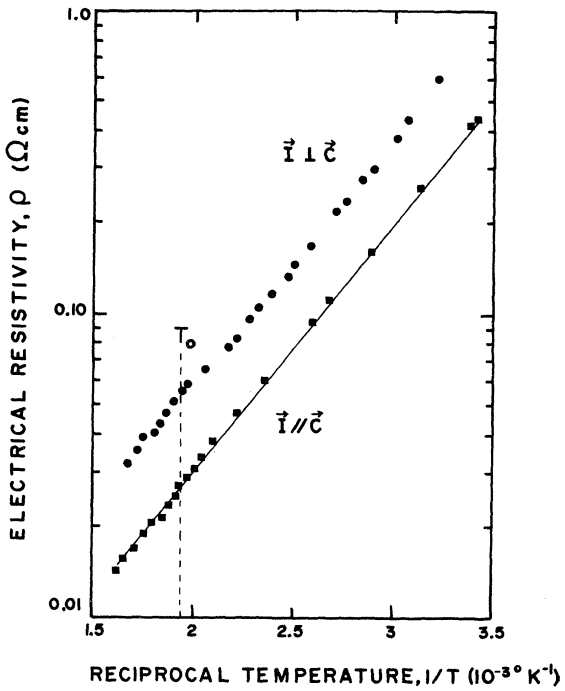

FIG. 2. Electrical resistivity of intrinsic tellurium samples plotted against reciprocal absolute temperature. The anomalous sign reversal of Hall coefficient takes place at temperature T_0. The line through the points for I parallel to c was calculated from the computed mobilities and carrier concentrations for the DCB model with $b_1 = 2.4$ and $b_2 = 0.05$.

III. TRANSPORT FORMULAS

A. Double-conduction-band (DCB) model

For an isotropic parabolic system of two conduction bands and one valence band [Fig. 5(a)], having mobilities μ_{n_1}, μ_{n_2}, and μ_p and carrier concentrations n_1, n_2, and p, respectively, the electrical conductivity σ, Hall coefficient R_H, and transverse magnetoresistance $\Delta\rho/\rho_0$ in weak magnetic fields (i.e., $\mu_n B \ll 1$, etc.) are given by

$$\sigma = e(n_1\mu_{n_1} + n_2\mu_{n_2} + p\mu_p), \tag{1}$$

$$R_H = r\,\frac{p\mu_p^2 - n_1\mu_{n_1}^2 - n_2\mu_{n_2}^2}{e(n_1\mu_{n_1} + n_2\mu_{n_2} + p\mu_p)^2}, \tag{2}$$

$$\frac{\Delta\rho}{\rho_0 B^2} = m\,\frac{n_1\mu_{n_1}^3 + n_2\mu_{n_2}^3 + p\mu_p^3}{n_1\mu_{n_1} + n_2\mu_{n_2} + p\mu_p} - (R_A\sigma)^2. \tag{3}$$

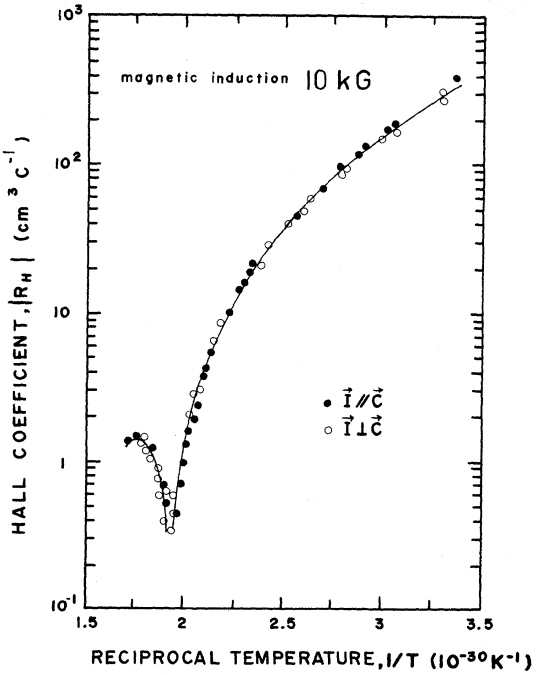

FIG. 3. Magnitude of the Hall coefficient in intrinsic tellurium samples plotted against reciprocal absolute temperature. The anomalous sign reversal is that shown. The line was calculated for the DCB model with $b_1=2.4$ and $b_2=0.05$.

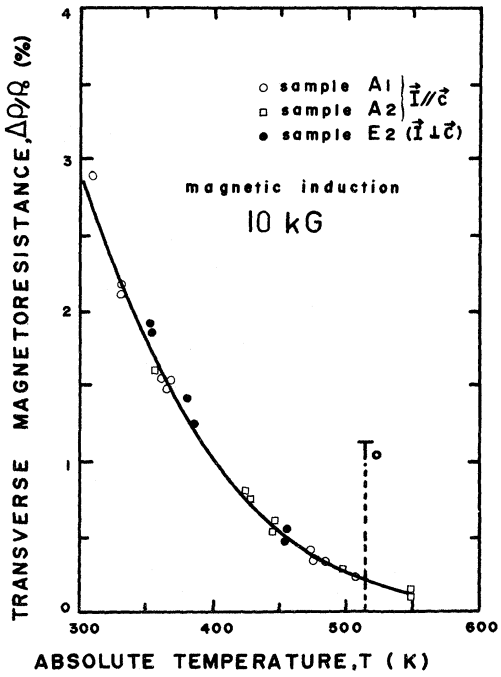

FIG. 4. Transverse magnetoresistance of intrinsic tellurium samples plotted against absolute temperature. The anomalous-sign-reversal temperature is indicated at T_0. The line was calculated for the DCB model with $b_1=2.4$ and $b_2=0.05$.

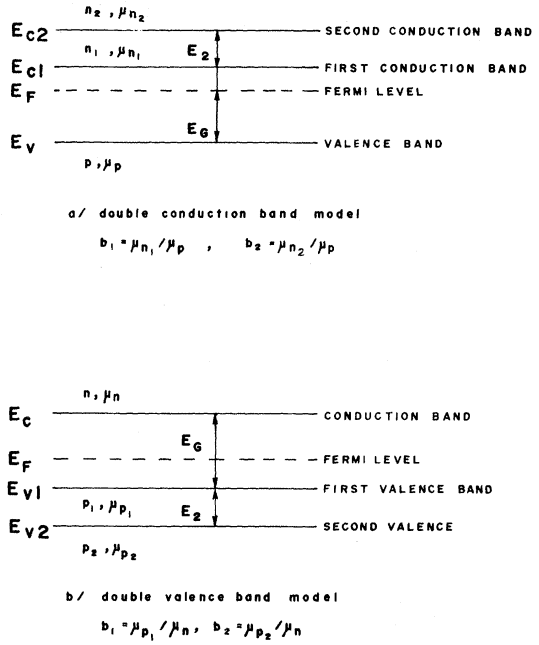

FIG. 5. Energy diagram of the two tri-band models used in the analysis of the experimental results.

In the intrinsic range, we also have

$$p=n_1+n_2. \tag{4}$$

With nondegenerate carrier concentrations, the coefficients r and m are given by

$$r=\frac{3\pi^{1/2}(2s+\frac{3}{2})!}{4[(s+\frac{3}{2})!]^2}, \tag{5}$$

$$m=r^2\frac{(3s+\frac{3}{2})!(s+\frac{3}{2})!}{[(2s+\frac{3}{2})!]^2}. \tag{6}$$

The parameter s is defined for a relaxation time assumed proportional to ϵ^s, where ϵ is the carrier energy. If mobility ratios are defined as

$$\mu_{n_1}/\mu_p=b_1, \tag{7}$$

$$\mu_{n_2}/\mu_p=b_2, \tag{8}$$

Eqs. (1)–(4) can be solved to give

$$\mu_p=\frac{R_H\sigma}{2r}\frac{b_1+b_2-1}{b_1+b_2-b_1b_2}\times\left\{\frac{|R_H|}{R_H}\left[1+4\frac{b_1+b_2-b_1b_2}{(b_1+b_2-1)^2}\times\left(\frac{\Delta\rho}{\rho_0(R_H\sigma B)^2}+1\right)\frac{r^2}{m}\right]^{1/2}+1\right\}, \tag{9}$$

$$n_1=\frac{\sigma}{e\mu_p}\frac{R_H\sigma/r\mu_p+b_2-1}{(b_2-b_1)(1+b_1)}, \tag{10}$$

$$p=\frac{\sigma}{e\mu_p}\,\frac{R_H\sigma/r\mu_p+b_1+b_2}{(1+b_1)(1+b_2)}\,, \tag{11}$$

$$n_2=p-n_1=\frac{\sigma}{e\mu_p}\,\frac{1-b_1-R_H\sigma/r\mu_p}{(b_2-b_1)(1+b_2)}\,. \tag{12}$$

To find the mobilities and carrier concentrations with Eqs. (9)–(12), values of b_1 and b_2 must be specified. To obtain a double reversal of Hall coefficient in the DCB model it is required that $\mu_{n_1}>\mu_p>\mu_{n_2}$ or $b_1>1>b_2$. However, all such values of b_1 and b_2 are not acceptable, since some give negative carrier concentrations, which have no physical meaning. Equations (10) and (12) show, in fact, that n_1 and n_2 are negative, unless

$$b_1>1-R_H\sigma/r\mu_p>b_2\,. \tag{13}$$

B. Double-valence-band (DVB) model

For an isotropic parabolic system of one conduction band and two valence bands [Fig. 5(b)], having mobilities μ_n, μ_{p_1}, and μ_{p_2} and carrier concentrations n, p_1, and p_2, respectively, the conductivity, Hall coefficient, and magnetoresistance are also given by Eqs. (1)–(4), if R_H is changed to $-R_H$, n to p, n_1 to p_1, n_2 to p_2, μ_{n_1} to μ_{p_1}, etc. With these changes, solutions (9)–(12) also apply, while the mobility ratios are now defined by

$$\frac{\mu_{p_1}}{\mu_n}=b_1\,, \tag{7a}$$

$$\frac{\mu_{p_2}}{\mu_n}=b_2\,. \tag{8a}$$

To obtain a double reversal of Hall coefficient with the DVB model, it is required that $\mu_{p_2}>\mu_n>\mu_{p_1}$ or $b_2>1>b_1$. To avoid meaningless negative values of p_1 and p_2, it is also required that

$$b_2>1+R_H\sigma/r\mu_n>b_1\,. \tag{13a}$$

IV. ANALYSIS OF RESULTS

An average set of σ, R_H, and $\Delta\rho/\rho_0$ values were obtained from the experimental results, and this was analyzed using the equations of Sec. III, assuming the mobility ratios b_1 and b_2 to be constant parameters over the whole measured range of temperature. The analysis was done with an IBM 360/75 computer. The coefficients r and m of Eqs. (5) and (6) were assigned the values 1.18 and 1.77, corresponding to acoustic lattice scattering ($s=-\frac{1}{2}$), but, apart from this, no assumption of a specific scattering mechanism was assumed elsewhere in the analysis.

A. Double-conduction-band model–First analysis

A computer program was first set up to calculate the carrier concentrations and mobilities for the DCB model using Eqs. (9)–(12) for specific pairs of values of b_1 and b_2. The program was then arranged to test the computed results against four rejection conditions, wherein the numerals 1, 2, 3, or 4 were printed out in a table of b_1 and b_2 values (Fig. 6) if at any measured temperature (1) n_1 was negative, (2) n_2 was negative, (3) p decreased with increasing temperature, or (4) n_2 decreased with temperature. It is shown in the appendix that p and n_2 must increase with temperature for the DCB model of Fig. 5(a). The sequence 1, 2, 3, 4, and blank was arranged to be in decreasing order of priority. For instance, a "1" excludes the higher numbers, so that conditions 2, 3, and 4 would not be tested. A "2" means "1" did not apply, "2" applied, but "3" and "4" were not examined. Blank spaces mean conditions 1, 2, 3, and 4 did not apply, so the b_1, b_2 values are acceptable. Ignoring for the moment the higher numbers in the computer printout of Fig. 6, it is seen

Numbers Representing Rejected Solutions for DCB Model

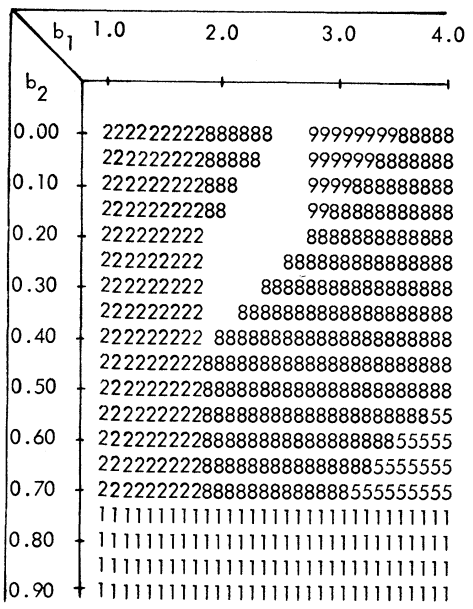

FIG. 6. Computer-generated table of numbers for the double-conduction-band model indicating where the following rejection conditions have been encountered. 1: n_1 is negative; 2: n_2 is negative; 3: p decreases with T; 4: n_2 decreases with T; 5: slope of $\ln\mu$ vs $\ln T$ is positive; 6: conditions 7 and 8 together; 7: slope $\ln\mu$ vs $\ln T$ less than -4; 8: calculated n_i differs from extrapolated n_i by more than 25%; 9: n_2 is greater than n_1 at room temperature. Priority decreases with increasing number.

that the 1's and 2's confine the mobility ratios to the values $b_1 > 1.8$, $b_2 < 0.75$. These arise from inequality (13).

B. Double-valence-band model–First analysis

A similar computer program was set up for the DVB model with the following rejection conditions: print 1 or 2, respectively, if p_1 or p_2 are negative, and print 3 or 4, respectively, if n or p_2 decreases with temperature. Ignoring the other numbers in Fig. 7, it is seen that the 1's and 2's restrict the mobility ratios to $b_1 < 0.56$ and $b_2 > 1.35$. These arise from inequality (13a).

C. Further rejection conditions

Since the first analysis restricted the range of b_1, b_2 values but did not indicate a preference for one model over the other, five extra rejection conditions were added to the computer program. For the DCB model these were

(5) If the smoothed-out μ_p value increases with temperature, print the numeral 5 for that particular pair of b_1, b_2 values. This rejection condition was included because some form of lattice scattering is expected in the intrinsic temperature range of measurement which should cause mobility to decrease with temperature.

(6) If conditions (7) and (8) both apply, print a 6. Since, this is a stronger ground for rejection than either (7) or (8) alone, it has a higher priority and hence a lower number.

(7) If, at any temperature, the smoothed-out curve of μ_p vs T decreases faster than T^{-4} [i.e., if $(T/\mu_p)(\Delta\mu_p/\Delta T) < -4$], print a 7.

(8) If the intrinsic carrier concentration $n_i = \sqrt{pn_1}$ [see Appendix, Eq. (A9)] differs from n_{ie} by more than 25% at any temperature, print an 8. Here, n_{ie} represents an intrinsic concentration extrapolated from room temperature and was specifically defined in the computer program as

$$n_{ie} = (pn_1)_{298\,\mathrm{K}}{}^{1/2}\left(\frac{T}{298}\right)^{3/2}\exp\left[-\frac{0.32}{2k}\left(\frac{1}{T}-\frac{1}{298}\right)\right],$$

with T in °K and k in eV/°K.

(9) If n_2 exceeds n_1 at room temperature, print a 9.

The computer print-out result in Fig. 6 shows that conditions (5), (8), and (9) eliminate many b_1, b_2 values, leaving a fairly small area of allowed values with the approximate ranges $1.8 < b_1 < 2.8$ and $1.0 - 0.3b_1 > b_2 > 0.75 - 0.3b_1$.

Corresponding rejection conditions were also added to the DVB-model computer program. The result in Fig. 7 shows that in this case all b_1, b_2 values were rejected, with the rectangular area bordered by 1's and 2's now filled almost entirely with 6's, showing that, for the most part, both conditions 7 and 8 applied.

Numbers Representing Rejected Solutions for DVB Model

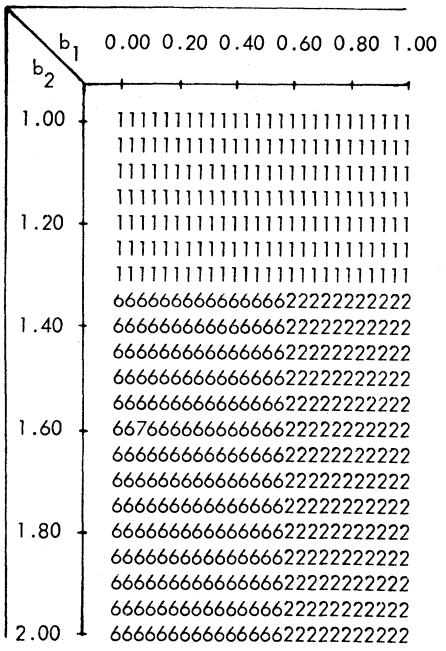

FIG. 7. Computer-generated table of numbers for the double-valence-band model indicating where the following rejection conditions have been encountered. 1: p_1 is negative; 2: p_2 is negative; 3: n decreases with T; 4: p_2 decreases with T; 5: slope of $\ln\mu$ vs $\ln T$ is positive; 6: conditions 7 and 8 together; 7: slope $\ln\mu$ vs $\ln T$ less than -4; 8: calculated n_i differs from extrapolated n_i by more than 25%; 9: p_2 is greater than p_1 at room temperature. Priority decreases with increasing number.

The difference in the two models, as far as mobility-temperature dependence is concerned, is illustrated in Figs. 8 and 9, where the logarithm of the mobility is plotted against $\ln T$. For the DVB case, the tangent to the steepest part of the curve corresponds to a dependence of the form T^n, with n less than -4.5 for all of the b_1, b_2 values examined (of course the complete range of b_1, b_2 values was examined by condition 7). This dependence is too steep to be accounted for by either acoustic or optical lattice scattering. Accordingly, because of this and the deviation from n_{ie}, the DVB model must be ruled out as physically inapplicable. The DCB model, on the other hand, (Fig. 9) gives mobility-temperature dependencies with n between -2.2 and -2.5, which is more consistent with what is found in other semiconductors. Hence the DCB scheme is the more acceptable

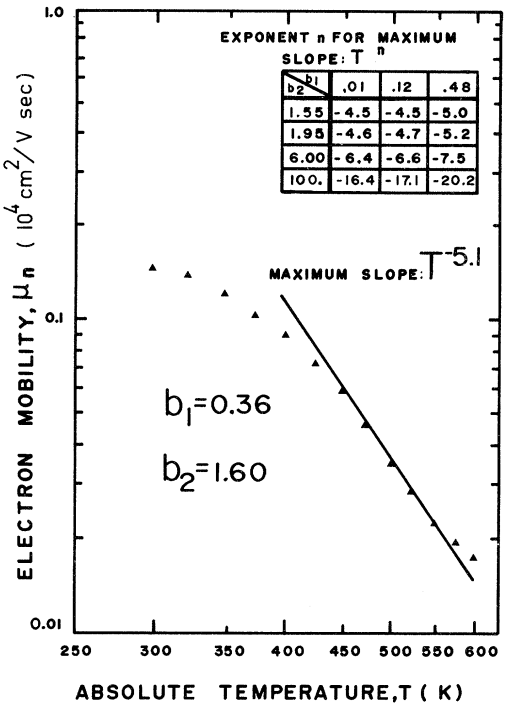

FIG. 8. Log-log plot of electron mobility against absolute temperature, calculated for the DVB model with the values of b_1 and b_2 shown.

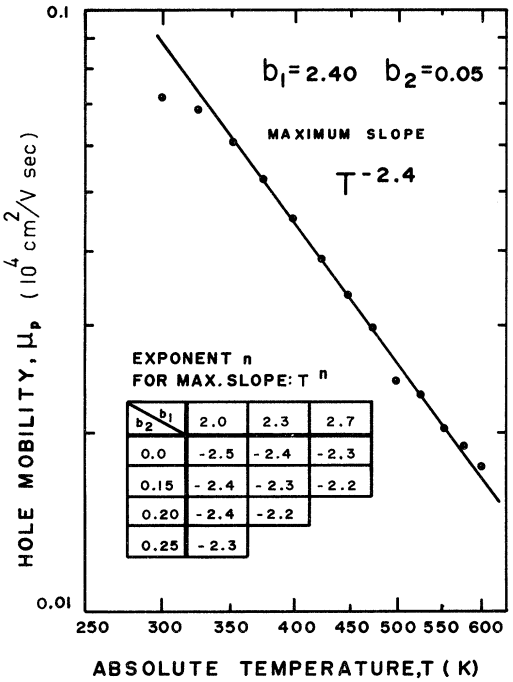

FIG. 9. Log-log plot of hole mobility against absolute temperature, calculated for the DCB model with the values of b_1 and b_2 shown.

model for explaining the observed intrinsic galvanomagnetic results.

D. Parameters for DCB model

It is shown in the Appendix [Eq. (A8)] that for the DCB model $n_2/n_1 = (m_2/m_1)^{3/2} e^{-E_2/kT}$. Thus in Fig. 10 a plot is made of $\ln(n_2/n_1)$ against $1/T$ for three pairs of b_1, b_2 values. The nearly horizontal portion of the curves near room temperature is due to the insensitivity of the results to the smaller electron population in the upper band at lower temperatures. The slopes of the straight lines drawn through the points at higher temperatures yield the E_2 values given in the inset of Fig. 10. With $b_1 = 2.4$ and $b_2 = 0.05$, for instance, E_2 is 0.36 eV and m_2/m_1 is 600.

V. DISCUSSION

The present analysis thus supports the conclusion of Rigaux[4] and Link[5] that the double-conduction-band model is more consistent with the measured transport properties than the double-valence-band model. Hence it appears that the known split-off H_5 valence band, situated approximately 0.13 eV[9] below the H_4 valence band, does not play

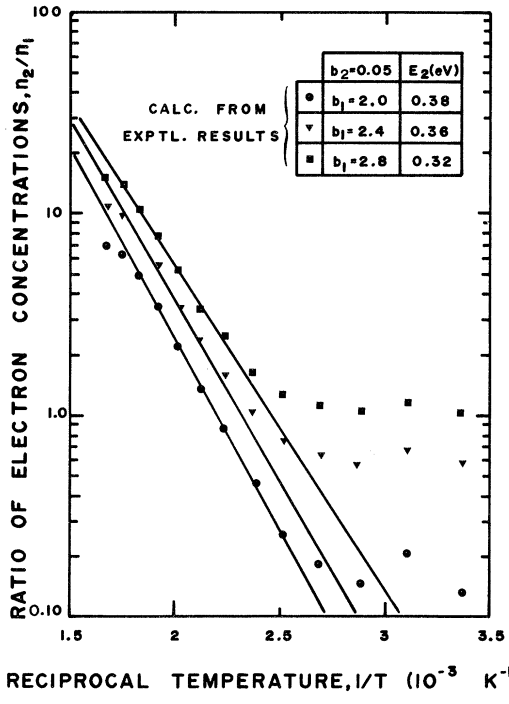

FIG. 10. Plot against reciprocal absolute temperature of the logarithm of the ratio of the electron concentration in the upper band (n_2) to that in the normal conduction band (n_1) calculated for the DCB model with the values of b_1 and b_2 shown.

a decisive role in the intrinsic region. It will of course make some contribution, but this cannot be assessed in the present method of analysis, since the inclusion of a fourth band introduces extra parameters. However, the effect of the H_5 valence band might be estimated by a synthesis in which the transport coefficients are calculated with and without the extra band and then compared, making reasonable assumptions for the band parameters and their dependencies on temperature.

Taking $b_1 = 2.4$ from Ref. 10, the present analysis gives $0 < b_2 < 0.3$. With $b_2 = 0.05$ for instance, we obtain $E_2 = 0.36$ eV and $m_2/m_1 = 600$. These values may be compared with $b_1 = 1.75$, $b_2 = 0.73$, $E_2 = 0.36$ eV, and $m_2/m_1 = 630$ of Rigaux[4] and also with $b_1 = 2.0$ and $b_2 = 0$ of Link.[5] Taking $m_2/m_1 = 600$ with $m_1/m_0 = 0.04$,[11] we get the effective mass ratio of $m_2/m_0 = 24$ for the upper band. High as this value is, it is not the infinite value which corresponds to Link's[5] postulated zero mobility for this band. While a level of localized centers arising from lattice defects might act like a nonconducting electron band, such a level was not confirmed by the fast-heating experiments of Link and Lutsch.[3] Thus the concept of a very flat upper conduction band remains. An effective mass ratio of 0.75 from cyclotron resonance was reported by Radoff and Dexter,[12] which they attributed to a higher conduction band. This mass ratio is much larger than the average value of 0.04[11] for the lower conduction band, but not high enough to fit the present results.

The presence of a conduction band some 0.36 eV above the normal conduction band would be expected to have some effect on reflectance spectra of tellurium. Tutihasi, Roberts, Keezer, and Drews[13] reported a small maximum in the imaginary dielectric constant at 0.7 eV from reflectance studies at 10 K. Further, Herwig, Stuke, and Weiser[14] found an electroreflectance peak at the same energy at 10 K. This they interpreted as a transition from a deeper lying valence band (H_6) to the normal conduction band (H_6). However, the energy could also be explained by a transition from the upper valence band (H_4) to the postulated upper conduction band, since $E_G + 0.36$ is approximately 0.7 eV, if E_G is taken as 0.335 eV.

While the normal conduction band minimum is situated at the H point of the Brillouin zone, the location of the upper conduction band is less certain. Inspection of the results of the band-structure calculations of Treusch and Sandrock[15] or Kramer and Thomas[16] suggests that the minima might be located at the Z or Γ points.

Some of the other limitations and assumptions in the analysis are now briefly discussed.

To simplify the analysis, anisotropy in the mobilities was not taken into account. A partial justification for this is the isotropy of the measured Hall coefficient and transverse magnetoresistance values in the intrinsic range.

The analysis was done with $r = 1.18$ and $m = 1.77$, corresponding to acoustic lattice scattering. These may not be the most appropriate values, since there are indications that polar optical scattering[17] may be important in tellurium. However, this is not yet established, particularly in view of the $T^{-2.4}$ mobility dependence shown in Fig. 9. In any case, the computer program is easily carried through for any value of r or m. With $r = m = 1$, corresponding to an energy-independent relaxation time ($s = 0$), it was found that the allowable range of b_1, b_2 values was not changed significantly.

It would seem that further refinement of b_1, b_2 values could be obtained by requiring a closer agreement than 25% of n_i to n_{ie}. However, this was not considered appropriate because of the effect of experimental errors on n_i and because the expression used for n_{ie} did not take into account variation of energy gap and effective masses with temperature. These dependencies are not known with any certainty in the intrinsic region.

A word of explanation is also needed for the apparently arbitrary assumption that n_2 is negligible in comparison with n_1 at room temperature. This is justified by the fact that the variation of $R_H\sigma$ with temperature in the range 250–350 K, for samples cut from tellurium of similar purity, can be satisfactorily explained with a simple two-band model.[10] Even when n_2 is equal to n_1, the contribution from the upper conduction band to terms such as $n_2\mu_{n_2}$, $n_2\mu_{n_2}^2$, and $n_2\mu_{n_2}^3$ in the transport coefficients is small, since $\mu_{n_2} \ll \mu_{n_1}, \mu_p$.

One of the most important assumptions in the analysis is that the mobility ratios are taken to be independent of temperature in the intrinsic range. This implies that the same lattice scattering mechanism holds for all three sets of carriers, which seems to be a reasonable assumption. It also implies that any variation of the effective masses with temperature for the three bands has the same functional form, but there appears to be no published evidence to support or deny this. In any case, some assumption of mobility ratio dependence on temperature must be made for the type of analysis given in this paper, and, in the absence of further information, constancy of values was the simplest assumption to make.

ACKNOWLEDGMENTS

The authors wish to acknowledge the support of this work by the National Research Council of Canada and by the Selenium-Tellurium Development Association, Inc.

APPENDIX

For the double-conduction-band model [Fig. 5(a)], the carrier concentrations expressed in terms of the Fermi level E_F, are given by

$$p = N_V e^{-(E_F - E_V)/kT}, \tag{A1}$$

$$n_1 = N_{c1} e^{-(E_{c1} - E_F)/kT}, \tag{A2}$$

$$n_2 = N_{c2} e^{-(E_{c2} - E_F)/kT}, \tag{A3}$$

$$p = n_1 + n_2, \tag{A4}$$

where

$$N_V = 2(2\pi m_p kT/h^2)^{3/2}, \tag{A5}$$

$$N_{c1} = 2(2\pi m_1 kT/h^2)^{3/2}, \tag{A6}$$

$$N_{c2} = 2(2\pi m_2 kT/h^2)^{3/2}, \tag{A7}$$

and m_p, m_1, and m_2 are the effective masses in the valence, first conduction, and second conduction bands, respectively.

Elimination of E_F from the above equations gives:

$$n_2/n_1 = N_{c2}/N_{c1} e^{-E_2/kT} = (m_2/m_1)^{3/2} e^{-E_2/kT}, \tag{A8}$$

$$pn_1 = N_V N_{c1} e^{-E_G/kT} = n_i^2, \tag{A9}$$

$$p = (N_{c1} N_V)^{1/2} e^{-E_G/2kT} [1 + (N_{c2}/N_{c1}) e^{-E_2/kT}]^{1/2}, \tag{A10}$$

$$n_1 = \frac{(N_{c1} N_V)^{1/2} e^{-E_G/2kT}}{[1 + (N_{c2}/N_{c1}) e^{-E_2/kT}]^{1/2}} = \frac{N_{c1}(N_V/N_{c2})^{1/2} e^{(E_2 - E_G)/2kT}}{[1 + (N_{c1}/N_{c2}) e^{E_2/kT}]^{1/2}}, \tag{A11}$$

$$n_2 = \frac{(N_{c2} N_V)^{1/2} e^{-(E_2 + E_G)/2kT}}{[1 + (N_{c1}/N_{c2}) e^{E_2/kT}]^{1/2}}. \tag{A12}$$

As T increases, Eqs. (A10) and (A12) show that p and n_2 always increase, but Eq. (A11) shows that n_1 increases only if $E_G > E_2$.

*Now at Université de Québec, Post Office Box 8888, Montreal 101, Québec, Canada.

[1] P. I. Wold, Phys. Rev. 7, 169 (1916).
[2] H. Fritzsche, Science 115, 571 (1952).
[3] R. Link and H. Lutsch, Phys. Status Solidi 26, K159 (1968).
[4] C. Rigaux, J. Phys. Chem. Solids 23, 805 (1962).
[5] R. Link, Phys. Status Solidi 12, 81 (1965).
[6] R. W. McKay and W. E. Gravelle, Can. J. Phys. 39, 534 (1961).
[7] P. Grosse, *Die Festkörpereigenschaften von Tellur* (Springer, New York, 1969), p. 116.
[8] T. Fukuroi, S. Tanuma, and S. Tobisawa, Sci. Rep. Res. Inst. Tohoku Univ. A 1, 373 (1949).
[9] D. Fischer, E. Bangert, and P. Grosse, Phys. Status Solidi B 55, 527 (1973).
[10] C. H. Champness and A. L. Kipling, Can. J. Phys. 48, 3038 (1970).
[11] P. Grosse and K. Winzer, Phys. Status Solidi 26, 139 (1968).
[12] P. L. Radoff and R. N. Dexter, Phys. Status Solidi 35, 261 (1969).
[13] S. Tutihasi, G. G. Roberts, R. C. Keezer, and R. E. Drews, Phys. Rev. 177, 1143 (1969).
[14] R. Herwig, J. Stuke, and G. Weiser, Phys. Status Solidi B 61, 521 (1974).
[15] J. Treusch and R. Sandrock, Phys. Status Solidi 16, 487 (1966).
[16] B. Kramer and P. Thomas, Phys. Status Solidi 26, 151 (1968).
[17] W. Hoerstel, D. Kurnick, and M. Spitzer, Phys. Status Solidi B 60, 213 (1973).